ACS OMEGA

http://pubs.acs.org/journal/acsodf

Article

# Photo-Fenton Process over an Fe-Free 3%-CuO/$Sr_{0.76}Ce_{0.16}WO_4$ Photocatalyst under Simulated Sunlight

Mingyan Fu, Jia Yang,* Xiaorui Sun,* Wei Tian, Guihua Yin, Sheng Tian, Mingdan Tan, Hongfu Liu, Xiaofeng Xing, and Huisheng Huang

Cite This: *ACS Omega* 2021, 6, 27297−27304

Read Online

ACCESS | Metrics & More | Article Recommendations | Supporting Information

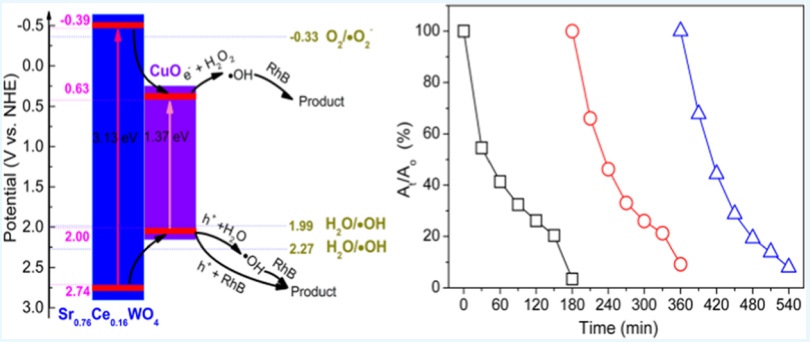


**ABSTRACT:** Photo-Fenton is a promising photocatalytic technology that utilizes sunlight. Herein, an Fe-free 3%-CuO/$Sr_{0.76}Ce_{0.16}WO_4$ photocatalyst was synthesized to apply simulated wastewater degradation via a photo-Fenton process under simulated sunlight. The photodegradation efficiency of RhB solution over the 3%-CuO/$Sr_{0.76}Ce_{0.16}WO_4$ photocatalyst is 93.2% in the first 3 h; its photocatalytic efficiency remains at 91.6% even after three cycle experiments. The kinetic constant of the 3%-CuO/$Sr_{0.76}Ce_{0.16}WO_4$ photocatalyst is 0.0127 $min^{-1}$, which is 2.8-fold that of an intrinsic $Sr_{0.76}Ce_{0.16}WO_4$ sample. The experiment of radical quenching revealed that the photogenerated electrons and holes are transferred to CuO to form hydroxyl radicals. Besides, the photocatalyst was characterized by scanning electron microscopy (SEM), Fourier transform infrared (FT-IR) spectroscopy, X-ray diffraction (XRD), diffused reflectance spectroscopy (DRS), and X-ray photoelectron spectroscopy (XPS) measurements. It has some reference significance for the design of iron-free photocatalysts.

## 1. INTRODUCTION

Environmental protection has been facing a huge challenge with the increasing development of industries,[1,2] i.e., printing and dyeing industry, leather tanning, pharmaceutical industry, petrochemical engineering, and so on. The organic content in wastewater as a harmful byproduct is generated in these industrial processes. It is necessary to remove contaminants via any advantageous method. The Fenton reaction is an effective method for the nonselective decomposition of organic pollutants, which is due to the powerful oxidation ability of hydroxyl radicals.[3,4] Faheem et al. reported $Cu_2O$-$CuFe_2O_4$ microparticles to degrade phenol at a pH of 4 in the presence of $H_2O_2$.[5] The Fenton agent is widely utilized for the degradation of organic content solutions. However, the reaction is only effective in an acidic aqueous environment.[6,7]

To eliminate the limitation of the pH value in the Fenton reaction, the photo-Fenton reaction was developed as a selective strategy for the decomposition of organic contaminants.[8,9] Generally, the Fe element is a key component of the catalyst that is utilized in the photo-Fenton reaction. For instance, without adjusting the pH value of the reaction solution, an $Fe_2O_3$-decorated $TiO_2$ nanotube shows an excellent methyl orange decomposition performance of 90% in 10 min.[10] When the initial pH value of rhodamine 6G is 6.9, a 1 wt % iron-containing $TiO_2$ photocatalyst displays almost complete color removal after 90 min of the photoreaction.[11] The $Bi_2Ga_{3.2}Fe_{0.8}O_9$ photocatalyst presents a nearly 100% photodegradation activity of RhB at neutral conditions.[12] The Fe element in the photocatalyst plays the role of an active site to facilitate the production of •OH. However, the possible existence of ferromagnetism may cause the photocatalyst to disperse unevenly in the solution via a magnetic agitator, which is unfavorable for the photocatalytic reaction.

Recently, an iron-free semiconducting material was utilized in the photo-Fenton reaction. A $ZnS/SnO_2$ nanosheet acts in

Received: August 1, 2021
Accepted: October 1, 2021
Published: October 10, 2021

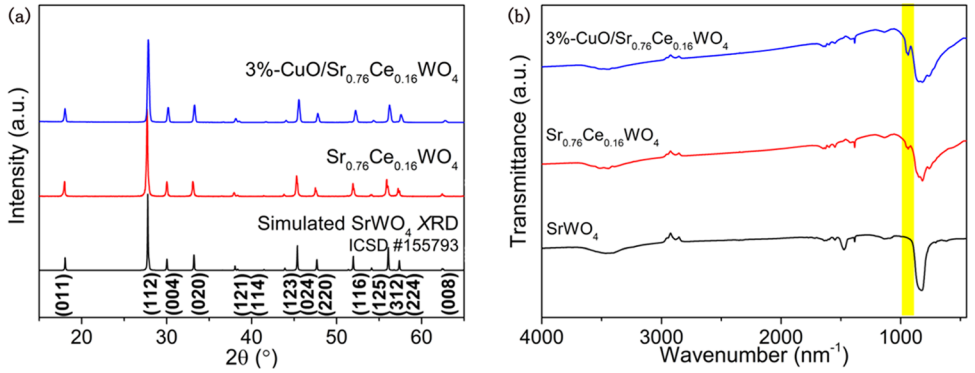


**Figure 1.** (a) Simulated XRD pattern of $SrWO_4$ and the powder XRD pattern of the $Sr_{0.76}Ce_{0.16}WO_9$ sample. (b) FT-IR spectra of $Sr_{0.76}Ce_{0.16}WO_4$ and $SrWO_4$.

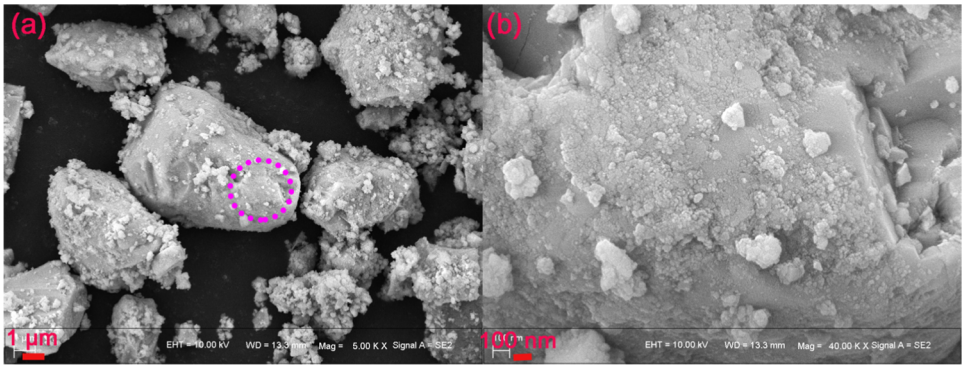


**Figure 2.** SEM images of the 3%-CuO/$Sr_{0.76}Ce_{0.16}WO_4$ photocatalyst in different scale plates: (a) 1 $\mu$m and (b) 100 nm.

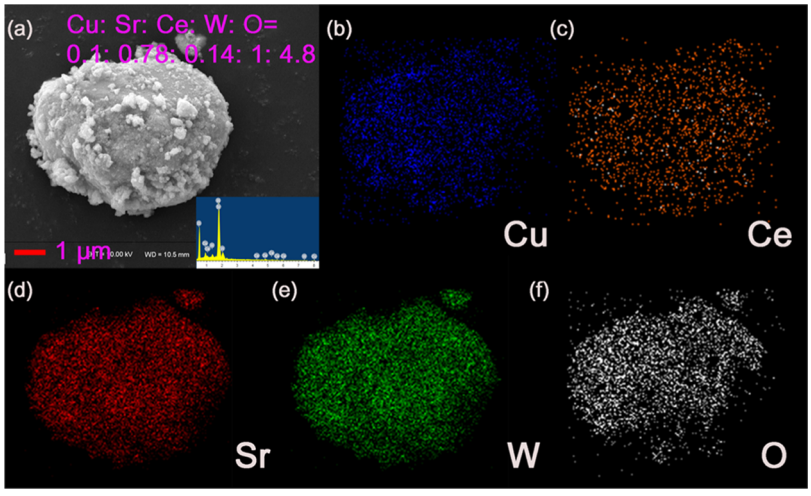


**Figure 3.** (a) EDS image of the 3%-CuO/$Sr_{0.76}Ce_{0.16}WO_4$ sample. (b–f) The mapping images for Cu, Ce, Sr, W, and O, respectively.

the degradation reaction of roxithromycin and clarithromycin antibiotics under ultraviolet light.[13] A supramolecular Cu-containing polymeric structure was synthesized for the degradation of naphthol blue black in water via the photo-Fenton process.[14] A series of $Cu_xP_2O_{5+x}$ ($x$ = 2, 3, 4) semiconducting materials were obtained via a traditional solid-state method, which were utilized in the photo-Fenton reaction for the first time under visible–infrared light irradiation.[15] Herein, an iron-free material, $Sr_{0.76}Ce_{0.16}WO_4$, was used as a photocatalyst for the photo-Fenton degradation of simulated wastewater. Four kinds of metal elements, CuO, Ag, Au, and Pt, were loaded on the as-prepared photocatalyst via the photodeposition method. A pseudo first-order kinetic constant was employed to quantitatively assess the photocatalytic performance of RhB.[16,17]

## 2. RESULTS AND DISCUSSION

Figure 1a shows that the $Sr_{0.76}Ce_{0.16}WO_4$ sample was successfully synthesized without any impurities compared to the simulated XRD pattern of $SrWO_4$.[18] The sample has high crystallinity, revealed by the sharp characteristic peak (112) and its high intensity. In addition, other diffraction peaks are consistent with the standard XRD pattern. Figure 1b displays the Fourier transform infrared (FT-IR) spectra of


https://doi.org/10.1021/acsomega.1c04107
ACS Omega 2021, 6, 27297−27304

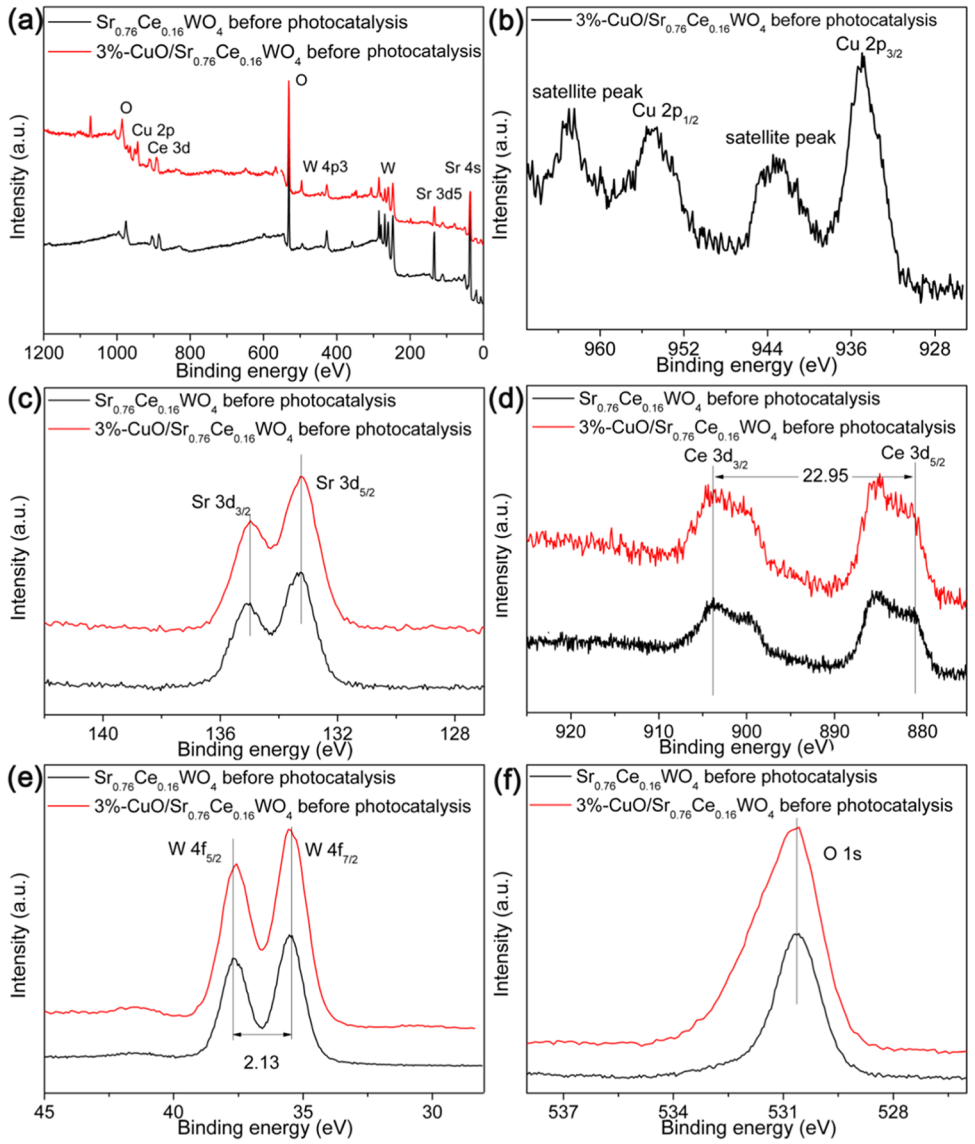


**Figure 4.** (a–f) XPS analysis of the measured spectra and high-resolution Cu 2p, Sr 3d, Ce 3d, W 4f, and O 1s in 3%-CuO/$Sr_{0.76}Ce_{0.16}WO_4$ and $Sr_{0.76}Ce_{0.16}WO_4$.

$Sr_{0.76}Ce_{0.16}WO_4$, which are compared with those of the undoped $SrWO_4$ sample. Pandey et al. studied the FT-IR spectra of the $Er^{3+}$–$Yb^{3+}$-codoped $SrWO_4$ sample,[19] which are similar to ours. Ju et al. reported that the characteristic peak of $Eu^{3+}$-doped $SrWO_4$ was at around 820 $nm^{-1}$.[20] In our experiment, the characteristic peak of $SrWO_4$ is at 834.2 $nm^{-1}$, which originates from the stretching mode of O–W–O in the $[WO_4]$ tetrahedron.[19,21] The peak (941.8 $nm^{-1}$) highlighted by the yellow rectangle shows the change after doping with Ce, which can help to indicate that Ce was successfully doped into the $SrWO_4$ sample. The higher the content of Ce, the more obvious this small peak is, and the characteristic peak with a wavenumber of 834.2 $nm^{-1}$ also appears to be a significant broadening phenomenon (see Figure S1a). In the crystal structure of $SrWO_4$, $Sr^{2+}$ is 8-fold coordinated and $W^{6+}$ is 4-fold coordinated. However, after Ce doping, the coordinate environment of $Sr^{2+}$ and $W^{6+}$ remains unchanged, but there are more 8-fold-coordinated Ce–O and Ce–O–W units in the crystal structure.[18] Therefore, the FT-IR spectra of $SrWO_4$, which originally had a single peak at 834 $nm^{-1}$, split into multiple peaks due to the introduction of Ce, which can be seen in the spectrum as the peak broadening. It should be pointed out that due to the low amount of CuO which is difficult to observe by XRD and FT-IR measurements.

Figure 2a displays that the $Sr_{0.76}Ce_{0.16}WO_4$ sample is composed of different scales of particles (0.2–8.5 $\mu$m). Figure 2b shows the smooth cross section of the sample, indicating good crystallization, consistent with XRD data. The nanoparticles around the surface of the cross section probably are Cu species. The energy-dispersive spectroscopy (EDS) data demonstrate that the average atomic ratio of Sr/Ce/W/O is 0.78:0.14:1:4.8 (see Figure 3a). Nevertheless, the Cu species were tested more than the loaded dosage, which may be because the low concentration of element is hard to detect accurately. Figure 3b–f shows that Cu, Sr, Ce, W, and O are uniformly dispersed on the surface layer of the 3%-CuO/$Sr_{0.76}Ce_{0.16}WO_4$ photocatalyst.

Figure 4 shows the XPS spectra of 3%-CuO/$Sr_{0.76}Ce_{0.16}WO_4$ in comparison with the unloaded $Sr_{0.76}Ce_{0.16}WO_4$ sample. Based on the previous SEM mapping results, the measurement


https://doi.org/10.1021/acsomega.1c04107
ACS Omega 2021, 6, 27297–27304

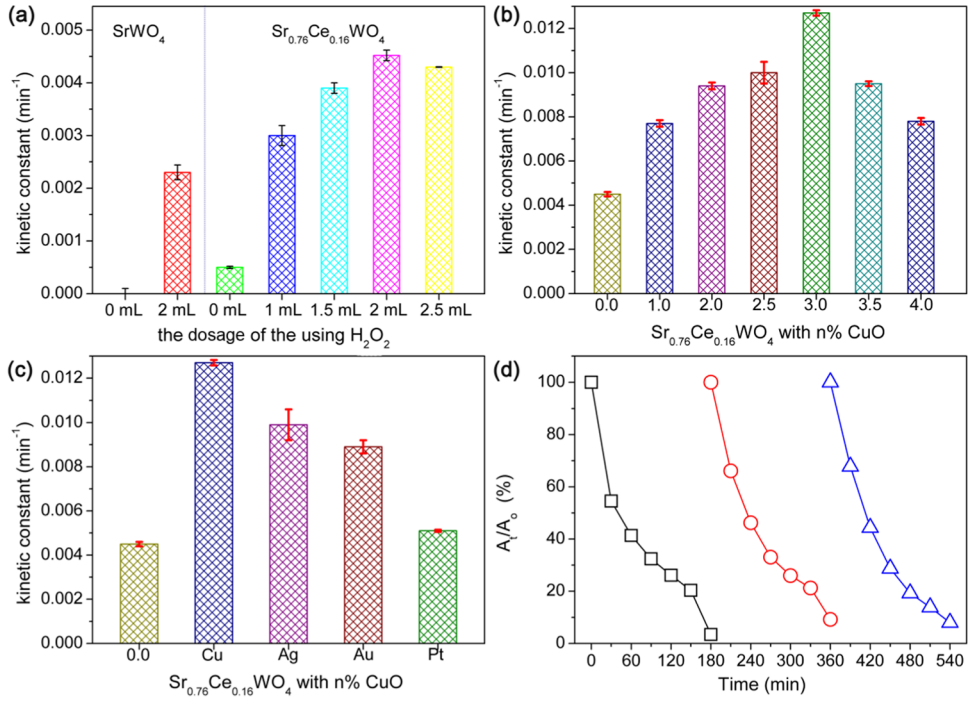


**Figure 5.** Kinetic constants of a differently univariate experiment: (a) the dosage of $H_2O_2$; (b) the amount of the loading CuO cocatalyst; (c) the 3% amount of different cocatalysts, and (d) the cyclic experiments of the 3%-CuO/$Sr_{0.76}Ce_{0.16}WO_4$ photocatalyst. Photocatalytic conditions: pH = 6.8, 0.1000 g of the photocatalyst, and 250 mL of the RhB solution (20 ppm).

spectra reconfirmed the presence of Cu, Ce, Sr, O, and W in the 3%-CuO/$Sr_{0.76}Ce_{0.16}WO_4$ photocatalyst (see Figure 4a). The specific type of Cu species cannot be identified by the SEM analysis. However, the chemical valence of the Cu element is +2, which was determined by the characteristic peaks of Cu $2p_{1/2}$ and $2p_{3/2}$ at 955.0 and 935.0 eV, respectively (see Figure 4b).[17,22,23] Hence, the Cu species is CuO. Figure 4c–e shows no change in the high-resolution Sr 3d, Ce 3d, and W 4f between the 3%-CuO/$Sr_{0.76}Ce_{0.16}WO_4$ and $Sr_{0.76}Ce_{0.16}WO_4$ samples. The valency of Sr was determined via the characteristic peaks of Sr $3d_{3/2}$ and $3d_{5/2}$ at 135.0 and 133.2 eV, respectively (see Figure 4c). The valency of Ce was determined via the characteristic peaks of Ce $3d_{3/2}$ and $3d_{5/2}$ at 903.8 and 880.8 eV, respectively (see Figure 4d).[24] The valency of W was determined via the characteristic peaks of W $3d_{5/2}$ and $3d_{7/2}$ at 37.7 and 35.4 eV, respectively (see Figure 4e). The chemical valences of $Sr^{2+}$, $Ce^{3+}$, and $W^{6+}$ were identified. The 1s band spectra of oxygen are ~529.7 and ~533.4 eV, generally considered surface lattice oxygen and chemisorbed oxygen, respectively.[21,25−30] The O 1s bands of Figure 4f are distributed at ~530.6 eV, a mixture of surface lattice oxygen and chemisorbed oxygen. The chemisorbed oxygen was dramatically increased by the influence of the CuO compound, which is different from the Au-loaded $Sr_{0.76}Ce_{0.16}WO_4$ sample (see Figure S2 and Table S1).

In this paper, the pH value of a 20 ppm RhB solution was adjusted by HCl and NaOH aqueous solutions. The results show that the absorbance of the RhB solution remains stable in a pH range from 1.2 to 10.6 (see Table S2). To avoid using extra acids and bases, a series of photo-Fenton experiments over modified $Sr_{0.76}Ce_{0.16}WO_4$ samples were performed in a neutral aqueous solution under sunlight irradiation. The $Sr_{0.76}Ce_{0.16}WO_4$ photocatalyst is the optimal one in comparison with the other Ce-doped $SrWO_4$ samples (see Figure S3). $H_2O_2$, which is the chief source of hydroxyl radicals, is a key factor in the photo-Fenton process.[31,32] Figure 5a presents the photocatalytic activities of $Sr_{0.76}Ce_{0.16}WO_4$ and $SrWO_4$ samples in the presence of different dosages of $H_2O_2$. The dosage of $H_2O_2$ exhibits a relatively optimal amount. Therefore, in the subsequent experiments in this paper, the amount of hydrogen peroxide was determined to be 1.5 mL. In our previous work, an inexpensive Cu species was utilized as a cocatalyst, which enhanced the photocatalytic activity.[12,17] Figure 5b shows that the optimal photocatalyst is 3%-CuO/$Sr_{0.76}Ce_{0.16}WO_4$. Furthermore, commensurable dosages of noble metal cocatalysts (Ag, Au, and Pt) were loaded on the $Sr_{0.76}Ce_{0.16}WO_4$ sample as a reference (see Figure 5c). Their kinetic constants are 0.0099, 0.0089, and 0.0051 $min^{-1}$ (see Table S3). In addition, there is no change in the FT-IR spectra of these samples after photocatalysis (see Figure S1b). The cyclic experiments were performed to detect the photostability of photocatalytic activity over the 3%-CuO/$Sr_{0.76}Ce_{0.16}WO_4$ photocatalyst, as shown in Figure 5d.[33] The photocatalytic performance of the 3%-CuO/$Sr_{0.76}Ce_{0.16}WO_4$ photocatalyst after 3 h is 93.2%. Even in the third cycle, the photocatalytic activity maintains a high value of 91.6%. Besides, no change is observed in the crystal structure of the 3%-CuO/$Sr_{0.76}Ce_{0.16}WO_4$ photocatalyst after the cyclic experiment (see Figure S4).

Since the toxicity of copper has a great influence on organisms and human health, the concentration of copper ions in the solution before and after a single illumination experiment was also measured. The experimental results show that the concentration of copper ions in the solution decreases a little after illumination (see Figure S5 and Table S3), probably within the error range, as a result of continued photoreduction of copper ions in the solution. The source of copper ions in the solution before illumination is because the supported cocatalyst has not been completely reduced in the set time. In conclusion, the results indicate that copper ions do not leach during photocatalysis.


https://doi.org/10.1021/acsomega.1c04107
ACS Omega 2021, 6, 27297−27304

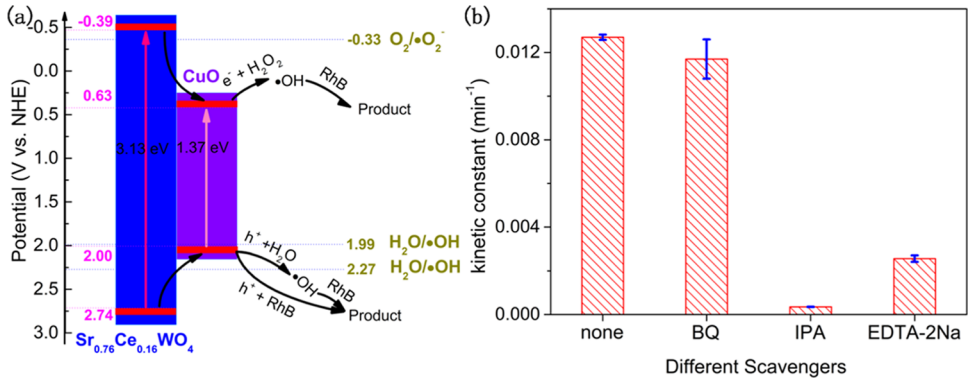


**Figure 6.** (a) Photo-oxidation RhB efficiency of 3%-CuO/$Sr_{0.76}Ce_{0.16}WO_4$ with different scavengers (1 mM). (b) The proposed photocatalytic mechanism over the CuO/$Sr_{0.76}Ce_{0.16}WO_4$ photocatalyst.

Finally, the photocatalytic mechanism was discussed to understand the photo-Fenton process without the presence of the Fe element. The potentials of the conduction band (CB) and the valence band (VB) are significant for analyzing the photocatalytic mechanism. There is a classical method that is called Mulliken electronegativity ($\chi$).[34,35] The applied equations are as follows

$$E_{VB} = \chi - E_e + 0.5E_g$$

$$E_{CB} = E_{VB} - E_g$$

where $E_{VB}$, $E_{CB}$, and $E_g$ are the VB potential, CB potential, and band gap of the photocatalyst, respectively; the magnitude of $E_e$ is 4.50 eV.[17] The $\chi$ values of $Sr_{0.76}Ce_{0.16}WO_4$ and CuO are 5.67 and 5.81 eV, respectively. The band gap of $Sr_{0.76}Ce_{0.16}WO_4$ is 3.13 eV (see Figure S6). The band gap of CuO nanoparticles is 1.37 eV. Hence, the $E_{CB}$ values of $Sr_{0.76}Ce_{0.16}WO_4$ and CuO are −0.39 and 0.63 V, respectively. The corresponding $E_{VB}$ values are 2.74 and 2.00 V. Based on these CB and VB potentials of $Sr_{0.76}Ce_{0.16}WO_4$ and CuO samples, a possible mechanism is shown in Figure 6a, which shows that •OH may play a major role in the photo-Fenton process. Then, three photocatalytic mechanism experiments for the detection of •OH, $•O_2^-$, and $H^+$ were carried out with isopropyl alcohol (IPA), *p*-benzoquinone (BQ), and ethylenediamine tetraacetic acid disodium (EDTA-2NA), respectively (see Figure 6b).[28,29,36−39] These photocatalytic results supported the proposed photocatalytic mechanism as well. In brief, when $Sr_{0.76}Ce_{0.16}WO_4$ and CuO are excited by simulated visible light, the photogenerated electrons and holes are obtained independently in them. Then, these photogenerated electrons move from the CB of $Sr_{0.76}Ce_{0.16}WO_4$ to the CB of CuO; meanwhile, the photogenerated holes move from the VB of $Sr_{0.76}Ce_{0.16}WO_4$ to the CB of CuO. Although the increase of available photogenerated carriers on CuO increases the probability of recombination, it provides the opportunity to improve the photocatalytic activity.

Because $E_{CB}(CuO) > E(O_2/•O_2^-)$, $•O_2^-$ cannot be produced in the CB of CuO, which is also consistent with the quenching experiment of free radicals; that is, superoxide anions have the least influence on the photocatalytic process. On the CB of CuO, the photogenerated electrons react with $H_2O_2$ to produce •OH. The photogenic holes clustered in the other half of the valence band can only oxidize water to form hydroxyl radicals due to the relationship of electric potential or directly oxidize pollutants. From the results of free radical quenching experiments, photogenerated holes tend to oxidize water to form hydroxyl radicals. This is also the reason for the sharp decrease in activity after the addition of IPA to the solution.

## 3. CONCLUSIONS

An iron-free material, 3%-CuO/$Sr_{0.76}Ce_{0.16}WO_4$, based on the photo-Fenton process, degrades simulated wastewater with RhB. The kinetic constant of the photocatalyst is 0.0127 $min^{-1}$, which is 2.8-fold that of an intrinsic $Sr_{0.76}Ce_{0.16}WO_4$ photocatalyst. The photocatalytic performance of the photocatalyst maintains stability in three cyclic experiments. The experiment of radical quenching reveals that •OH plays a major in the photo-Fenton process. The photogenerated electrons react with $H_2O_2$ to form •OH. The photogenerated holes react with $H_2O$ to form •OH as well. Photo-Fenton experiments can still be carried out efficiently without iron.

## 4. EXPERIMENTAL SECTION

**4.1. Synthesis of the Photocatalyst.** The $Sr_{0.76}Ce_{0.16}WO_4$ sample was obtained via a solid-state method at a high temperature. In a run, to obtain 1.3000 g of the sample, 0.3926 g of $SrCO_3$, 0.8111 g of $WO_3$, and 0.0963 g of $CeO_2$ were mixed evenly by hand. The mixture was first preheated at 700 °C for 10 h and finally heated at 1000 °C for 15 h in a high-temperature box furnace. After the preheating and heating processes, the obtained powders were ground adequately for half an hour. $Sr_{1-1.5x}Ce_xWO_4$ ($0 \le \times \le 0.20$) solid solutions were synthesized by the same method.

**4.2. Loading Cocatalyst.** The cocatalysts, CuO, Ag, Au, and Pt, were loaded on the $Sr_{0.76}Ce_{0.16}WO_4$ sample for improving its photocatalytic activity. For instance, 3%-CuO/$Sr_{0.76}Ce_{0.16}WO_4$ means loading 3.0 wt % Cu element on the $Sr_{0.76}Ce_{0.16}WO_4$ sample via the photodeposition method.[17] One hundred milligrams of the $Sr_{0.76}Ce_{0.16}WO_4$ powder sample and 9.42 mL of a 0.3182 mg/mL $Cu(CH_3COO)_2$ solution were mixed in 10 mL of a 10 vol % methanol solution. The mixture was mixed evenly via ultrasound treatment for 10 min. After that, the suspension solution was irradiated using a 300 W Hg lamp for 1 h. Finally, the obtained powder was dried in a drying oven at 65 °C and named 3%-CuO/$Sr_{0.76}Ce_{0.16}WO_4$.

**4.3. Characterization.** Powder X-ray diffraction (XRD) data were measured via a PANalytical X'pert diffractometer with Cu K$\alpha$ radiation. Fourier transform infrared spectroscopy (FT-IR, PerkinElmer Spectrum 100) was adopted to determine the structure information of the photocatalyst.


https://doi.org/10.1021/acsomega.1c04107
ACS Omega 2021, 6, 27297−27304

Scanning electron microscopy (SEM) and energy-dispersive spectroscopy (EDS) were performed on a ZEISS MERLIN Compact and an X-MAX-20 $mm^2$ attachment, respectively. The ultraviolet−visible diffused reflectance spectrum (DRS) was recorded using a Hitachi U-4100 spectrometer equipped with an integrating sphere accessory that used a $BaSO_4$ cylinder as a reflectance standard. X-ray photoelectron spectroscopy (XPS) was performed on a Thermo Fisher ESCALAB 250Xi with Al X-ray. The concentration of copper ions in the solution was determined by copper reagent spectrophotometry.

**4.4. Photocatalysis.** Photodegradation RhB activities were determined on a self-made device. In an experimental process, 100 mg of the photocatalyst was dispersed evenly in 250 mL of an aqueous solution containing 20 ppm RhB and 1.5 mL of $H_2O_2$ using a magnetic stirrer for 30 min. Before simulated sunlight irradiation, 5 mL of the solution was collected as a sample. After that, six samples were collected at 10 min intervals in the 1 h photocatalytic process. The heat generated by simulated sunlight irradiation was removed by circulating water at 20 °C. The absorption of the total seven samples was determined using a Hitachi U-4100 spectrometer. The photodegradation RhB activity was assessed as follows[12,4012,40]

$$\text{photodegradation RhB efficiency} = (A_0 - A_6)/A_0 \times 100\%$$

where $A_0$ means the absorption of the first sample before simulated sunlight irradiation, $A_6$ means the absorption of the last sample after simulated sunlight irradiation.

Kinetic constant $k$ can be calculated by the following equation[17,40]

$$\ln(A_0/A_6) = kt$$

## ■ ASSOCIATED CONTENT

### Supporting Information

The Supporting Information is available free of charge at https://pubs.acs.org/doi/10.1021/acsomega.1c04107.

Summary of the photo-oxidation RhB activity of the as-prepared photocatalyst; O 1s orbital composition of $Sr_{0.76}Ce_{0.16}WO_4$ and 3%-CuO/$Sr_{0.76}Ce_{0.16}WO_4$ samples are based on the analysis of XPS data; summary of the absorbance of a 20 ppm RhB solution at different pH values; absorbance and concentration of copper ions before and after the photocatalytic reaction were measured by copper reagent spectrophotometry; XRD image of the 3%-CuO/$Sr_{0.76}Ce_{0.16}WO_4$ sample after the cyclic experiment; DRS image of the $Sr_{0.76}Ce_{0.16}WO_4$ sample; and (a) FT-IR spectra of $Sr_{1-1.5x}Ce_xWO_4$ solid solutions and (b) FT-IR spectra of $Sr_{0.76}Ce_{0.16}WO_4$, which loaded different cocatalysts after photocatalysis (PDF)

## ■ AUTHOR INFORMATION


### Corresponding Authors

**Jia Yang** − *Chongqing Key Laboratory of Inorganic Special Functional Materials, College of Chemistry and Chemical Engineering, Yangtze Normal University, Fuling, Chongqing 408100, P. R. China;* orcid.org/0000-0001-7404-096X; Phone: +86-18716372096; Email: yangjiayznu@163.com

**Xiaorui Sun** − *Chongqing Key Laboratory of Inorganic Special Functional Materials, College of Chemistry and Chemical Engineering, Yangtze Normal University, Fuling, Chongqing 408100, P. R. China;* orcid.org/0000-0002-1715-4060; Phone: +86-18883876787; Email: sunxiaoruiyznu@163.com

### Authors

**Mingyan Fu** − *Chongqing Key Laboratory of Inorganic Special Functional Materials, College of Chemistry and Chemical Engineering, Yangtze Normal University, Fuling, Chongqing 408100, P. R. China*

**Wei Tian** − *Chongqing Key Laboratory of Inorganic Special Functional Materials, College of Chemistry and Chemical Engineering, Yangtze Normal University, Fuling, Chongqing 408100, P. R. China*

**Guihua Yin** − *Chongqing Key Laboratory of Inorganic Special Functional Materials, College of Chemistry and Chemical Engineering, Yangtze Normal University, Fuling, Chongqing 408100, P. R. China*

**Sheng Tian** − *Chongqing Key Laboratory of Inorganic Special Functional Materials, College of Chemistry and Chemical Engineering, Yangtze Normal University, Fuling, Chongqing 408100, P. R. China*

**Mingdan Tan** − *Chongqing Key Laboratory of Inorganic Special Functional Materials, College of Chemistry and Chemical Engineering, Yangtze Normal University, Fuling, Chongqing 408100, P. R. China*

**Hongfu Liu** − *Chongqing Key Laboratory of Inorganic Special Functional Materials, College of Chemistry and Chemical Engineering, Yangtze Normal University, Fuling, Chongqing 408100, P. R. China*

**Xiaofeng Xing** − *Chongqing Key Laboratory of Inorganic Special Functional Materials, College of Chemistry and Chemical Engineering, Yangtze Normal University, Fuling, Chongqing 408100, P. R. China*

**Huisheng Huang** − *Chongqing Key Laboratory of Inorganic Special Functional Materials, College of Chemistry and Chemical Engineering, Yangtze Normal University, Fuling, Chongqing 408100, P. R. China*

Complete contact information is available at: https://pubs.acs.org/10.1021/acsomega.1c04107


### Notes

The authors declare no competing financial interest.

## ■ ACKNOWLEDGMENTS

This work was financially supported by Chongqing Municipal Education Commission (KJQN202101405 and CXQT20026) and Talent Introduction Project of Yangtze Normal University (2017KYQD22). The authors would like to thank Ting Du from Shiyanjia Lab (www.shiyanjia.com) for SEM analysis.

## ■ REFERENCES

(1) Lam, S. S.; Nguyen, V.; Dinh, M. T. N.; Khieu, D. Q.; La, D. D.; Nguyen, H. T.; Vo, D. V. N.; Xia, C.; Varma, R. S.; Shokouhimehr, M.; et al. Mainstream avenues to boost graphitic carbon nitride efficiency: Toward enhanced solar-driven photocatalytic hydrogen production and environmental remediation. *J. Mater. Chem. A* **2020**, *8*, 10571−10603.

(2) Lang, X.; Ma, W.; Chen, C.; Ji, H.; Zhao, J. Selective aerobic oxidation mediated by $TiO_2$ photocatalysis. *Acc. Chem. Res.* **2014**, *47*, 355−363.

(3) Garcia-Segura, S.; Bellotindos, L. M.; Huang, Y.; Brillas, E.; Lu, M. Fluidize d-b e d Fenton process as alternative wastewater treatment technology-A review. *J. Taiwan Inst. Chem. Eng.* **2016**, *67*, 211−225.
(4) Bello, M. M.; Raman, A. A. A.; Asghar, A. A review on approaches for addressing the limitations of Fentonoxidation for recalcitrant wastewater treatment. *Process. Saf. Environ.* **2019**, *126*, 119−140.
(5) Faheem, M.; Jiang, X.; Wang, L.; Shen, J. Synthesis of $Cu_2O$−$CuFe_2O_4$ microparticles from Fenton sludge and its application in the Fenton process: the key role of $Cu_2O$ in the catalytic degradation of phenol. *RSC Adv.* **2018**, *8*, 5740−5748.
(6) Lu, H.; Chen, H.; Kao, C.; Chao, I.; Chen, H. Computational study of the Fenton reaction at 1 different pH ranges. *Phys. Chem. Chem. Phys.* **2018**, *20*, 22890−22901.
(7) Jeong, J.; Yoon, J. pH effect on OH radical production in photo/ferrioxalate system. *Water Res.* **2005**, *39*, 2893−2900.
(8) Zhu, Y.; Zhu, R.; Xi, Y.; Zhu, J.; Zhu, G.; He, H. Strategies for enhancing the heterogeneous Fenton catalytic reactivity: A review. *Appl. Catal., B* **2019**, *255*, 117739−117754.
(9) Zhang, M.; Dong, H.; Zhao, L.; Wang, D.; Meng, D. A review on Fenton process for organic wastewater treatment based on optimization perspective. *Sci. Total Environ.* **2019**, *670*, 110−121.
(10) Peng, Q.; Peng, G.; Wu, L.; Chen, Y.; Han, B.; Su, Q.; Liu, S.; Li, X. Photo-reduction enables catalysts regeneration in Fenton reaction on $Fe_2O_3$ decorated $TiO_2$ nanotube-based photocatalyst. *Dalton Trans.* **2020**, *49*, 6730−6737.
(11) Demir, N.; Gündüz, G.; Dükkanci, M. Degradation of a textile dye, Rhodamine 6G (Rh6G), by heterogeneous sonophotoFenton process in the presence of Fe-containing $TiO_2$ catalysts. *Environ. Sci. Pollut. Res.* **2015**, *22*, 3193−3201.
(12) Yang, J.; Sun, X.; Zeng, C.; Wang, X.; Hu, Y.; Zeng, T.; Shi, J. Highly improved photocatalytic degradation of rhodamine B over $Bi_2Ga_{4-x}FexO_9$ solid solutions under visible light irradiation. *RSC Adv.* **2019**, *9*, 26894−26901.
(13) Hosseini, M.; Kahkha, M. R. R.; Fakhri, A.; Tahami, S.; Lariche, M. J. Degradation of macrolide antibiotics via sono or photo coupled with Fenton methods in the presence of ZnS quantum dots decorated $SnO_2$ nanosheets. *J. Photochem. Photobiol., B* **2018**, *185*, 24−31.
(14) Mestivier, M.; Li, J. R.; Camy, A.; Frangville, C.; Mingotaud, C.; Benoît-Marquié, F.; Marty, J. Copper based hybrid polyion complexes for Fenton like rReactions. *Chem. - Eur. J.* **2020**, *26*, 14152−14158.
(15) Han, G. S.; Cho, I. S. Copper phosphate compounds with visible-to-near-infrared-active photo-Fenton-like photocatalytic properties. *J. Am. Ceram. Soc.* **2020**, *103*, 5120−5128.
(16) Zhang, L.; Shan, B.; Yang, H.; Wu, D.; Zhu, R.; Nie, J.; Cao, R. A new heterogeneous photocatalyst based on Wells−Dawson polyoxometalate and nickel coordination compounds: synthesis, structure and property. *RSC Adv.* **2015**, *5*, 23556−23562.
(17) Yang, J.; Fu, M.; Liu, H.; Yin, G.; Tan, M.; Sun, X.; Huang, H. An inexpensive CuO nanoparticles as cocatalyst significantly enhanced the photo-oxidation performance of $Bi_2Ga_{2.8}Al_{1.2}O_9$ photocatalyst under visible-light. *Mater. Lett.* **2021**, *283*, 128796−128799.
(18) Yang, J.; Sun, X.; Wang, R.; Zhu, M.; Yang, W.; Huang, H.; Shi, W. An Au-nanoparticle decorated $Sr_{0.76}Ce_{0.16}WO_4$ photocatalyst for $H_2$ evolution under visible-light irradiation. *Int. J. Hydrogen Energy* **2020**, *45*, 12702−12710.
(19) Pandey, A.; Rai, V. K.; Kumar, V.; Kumar, V.; Swart, H. C. Upconversion based temperature sensing ability of $Er^{3+}$-$Yb^{3+}$ codoped $SrWO_4$: An optical heating phosphor. *Sens. Actuators, B* **2015**, *209*, 352−358.
(20) Ju, Z.; Wei, R.; Gao, X.; Liu, W.; Pang, C. Red phosphor $SrWO_4$:$Eu^{3+}$ for potential application in white LED. *Opt. Mater.* **2011**, *33*, 909−913.
(21) Xie, X.; Hassan, Q. U.; Rao, F.; Gao, J.; Zhu, G.; et al. In situ construction of oxygen-vacancy-rich $Bi_0$@$Bi_2WO_{6-x}$ microspheres with enhanced visible light photocatalytic for NO removal. *Chin. Chem. Lett.* **2021**, *32*, 2038−2042.
(22) Le Minh Tri, N.; Trung, D. Q.; Thuan, D. V.; Cam, N. T. D.; Tahtamouni, T. A.; Pham, T.; Duc, D. S.; Tung, M. H. T.; Ha, H. V.; Thu, N. H. A.; Trang, H. T. The advanced photocatalytic performance of V doped $CuWO_4$ for water splitting to produce hydrogen. *Int. J. Hydrogen Energy* **2020**, *45*, 18186−18194.
(23) Liu, L.; Ji, Z.; Zou, W.; Gu, X.; Deng, Y.; Gao, F.; Tang, C.; Dong, L. In situ loading transition metal oxide clusters on $TiO_2$ nanosheets as co-catalysts for exceptional high photoactivity. *ACS Catal.* **2013**, *3*, 2052−2061.
(24) Nie, J.; Zhu, G.; Zhang, W.; Gao, J.; Zhong, P.; Xie, X.; Huang, Y.; Hpjamberdiev, M. Oxygen vacancy defects-boosted deep oxidation of NO by $\beta$-$Bi_2O_3$/$CeO_{2-\delta}$ p-n heterojunction photocatalyst in situ synthesized from $Bi/Ce(CO_3)(OH)$ precursor. *Chem. Eng. J.* **2018**, *424*, No. 130327.
(25) Hammond, J. S.; Holubka, J. W.; Devries, J. E.; Dickie, R. A. The application of x-ray photo-electron spectroscopy to a study of interfacial composition in corrosion-induced paint de-adhesion. *Corros. Sci.* **1981**, *21*, 239−253.
(26) Lei, L.; Shi, J.; Wang, X.; Liu, D.; Xu, H. Microstructure and electrochemical behavior of cerium conversioncoating modified with silane agent on magnesium substrates. *Appl. Surf. Sci.* **2016**, *376*, 161−171.
(27) Li, S.; Wang, C.; Cai, M.; Yang, F.; Liu, Y.; Chen, J.; Zhang, P.; Li, X.; Chen, X. Facile fabrication of TaON/$Bi_2MoO_6$ core-shell S-scheme heterojunction nanofibers for boosting visible-light catalytic levofloxacin degradation and Cr(VI) reduction. *Chem. Eng. J.* **2022**, *428*, No. 131158.
(28) Ou, Y.; Zhu, G.; Rao, F.; Gao, J.; Chang, J.; Xie, T.; Zhang, W.; Huang, Y.; Hojamberdiece, M. Coral-shaped $TiO_{2-\delta}$ decorated with carbon quantum dots and carbon nanotubes for NO removal. *ACS Appl. Nano Mater.* **2021**, *4*, 7330−7342.
(29) Guo, T.; Wang, K.; Zhang, G.; Wu, X. A novel $\alpha$-$Fe_2O_3$@g-$C_3N_4$ catalyst: Synthesis derived from Fe-based MOF and its superior photo-Fenton performance. *Appl. Surf. Sci.* **2019**, *469*, 331−339.
(30) Huang, H.; Guo, T.; Wang, K.; Li, Y.; Zhang, G. Efficient activation of persulfate by a magnetic recyclable rape straw biochar catalyst for the degradation of tetracycline hydrochloride in water. *Sci. Total Environ.* **2021**, *758*, No. 143957.
(31) Kaynan, N.; Berke, B. A.; Hazut, O.; Yerushalmi, R. Sustainable photocatalytic production of hydrogen peroxide from water and molecular oxygen. *J. Mater. Chem. A* **2014**, *2*, 13822−13826.
(32) Shiraishi, Y.; Kanazawa, S.; Kofuji, Y.; Sakamoto, H.; Ichikawa, S.; Tanaka, S.; Hirai, T. Sunlight-driven hydrogen peroxide production from water and molecular oxygen by metal-free photocatalysts. *Angew. Chem., Int. Ed.* **2014**, *53*, 13454−13459.
(33) Guo, T.; Jiang, L.; Wang, K.; Li, Y.; Huang, H.; Wu, X.; Zhang, G. Efficient persulfate activation by hematite nanocrystals for degradation of organic pollutants under visible light irradiation: Facet-dependent catalytic performance and degradation mechanism. *Appl. Catal., B* **2021**, *286*, No. 119883.
(34) Liu, J. J.; Fu, X. L.; Chen, S. F.; Zhu, Y. F. Electronic structure and optical properties of $Ag_3PO_4$ photocatalyst calculated by hybrid density functional method. *Appl. Phys. Lett.* **2011**, *99*, 191903−191905.
(35) Kong, L.; Guo, J.; Makepeace, J. W.; Xiao, T.; Greer, H. F.; Zhou, W.; Jiang, Z.; Edwards, P. P. Rapid synthesis of BiOBrxI1-x photocatalysts: Insights to the visiblelight photocatalytic activity and strong deviation from Vegard's Law. *Catal. Today* **2019**, *335*, 477−484.
(36) Lu, Z.; Yu, Z.; Dong, J.; Song, J.; Liu, Y.; Liu, X.; Ma, Z.; Su, H.; Yan, Y.; Huo, P. Facile microwave synthesis of a Z-scheme imprinted $ZnFe_2O_4$/Ag/PEDOT with the specific recognition ability towards improving photocatalytic activity and selectivity for tetracycline. *Chem. Eng. J.* **2018**, *337*, 228−241.
(37) Zhang, X.; Zhang, J.; Yu, J.; Zhang, Y.; Cui, Z.; Sun, Y.; Hou, B. Fabrication of $InVO_4$/$AgVO_3$ heterojunctions with enhanced photocatalytic antifouling efficiency under visible-light. *Appl. Catal., B* **2018**, *220*, 57−66.


https://doi.org/10.1021/acsomega.1c04107
*ACS Omega* 2021, 6, 27297−27304

(38) Asadzadeh-Khaneghah, S.; Habibi-Yangjeh, A.; Abedi, M. Decoration of carbon dots and AgCl over g-$C_3N_4$ nanosheets: Novel photocatalysts with substantially improved activity under visible light. *Sep. Purif. Technol.* **2018**, *199*, 64−77.
(39) Wan, Z.; Zhang, G.; W, X.; Yin, S. Novel visible-light-driven Z-scheme $Bi_{12}GeO_{20}$/g-$C_3N_4$ photocatalyst:Oxygen-induced pathway of organic pollutants degradation andproton assisted electron transfer mechanism of Cr(VI) reduction. *Appl. Catal., B*, **2017**, *207*, 17−26.
(40) Yang, J.; Fu, M.; Tan, M.; Tian, Y.; Sun, X.; Huang, H. Photocatalytic reduction of Cr(VI) on a 3.0% Au/$Sr_{0.70}Ce_{0.20}WO_4$ photocatalyst. *ACS Omega* **2020**, *5*, 26755−26762.


https://doi.org/10.1021/acsomega.1c04107
*ACS Omega* 2021, 6, 27297−27304